Exploring the importance of quantum effects in nucleation: The archetypical Nen case

Wesley Unn-Toc, Nadine Halberstadt, Christoph Meier, and Massimo Mella

Citation: J. Chem. Phys. **137**, 014304 (2012); doi: 10.1063/1.4730033
View online: http://dx.doi.org/10.1063/1.4730033
View Table of Contents: http://jcp.aip.org/resource/1/JCPSA6/v137/i1
Published by the American Institute of Physics.

Additional information on J. Chem. Phys.

Journal Homepage: http://jcp.aip.org/
Journal Information: http://jcp.aip.org/about/about_the_journal
Top downloads: http://jcp.aip.org/features/most_downloaded
Information for Authors: http://jcp.aip.org/authors

ADVERTISEMENT

Downloaded 02 Jul 2012 to 193.205.162.64. Redistribution subject to AIP license or copyright; see http://jcp.aip.org/about/rights_and_permissions

Exploring the importance of quantum effects in nucleation: The archetypical Ne_n case

Wesley Unn-Toc,[1] Nadine Halberstadt,[1] Christoph Meier,[1] and Massimo Mella[2,a)]
[1]*Laboratoire Collisions Agrégats Réactivité–IRSAMC, Université Paul Sabatier, 118 Route de Narbonne, 31062 Toulouse, France*
[2]*Dipartimento di Scienze Chimiche ed Ambientali, Università degli Studi dell'Insubria, via Lucini 3, 22100 Como, Italy*

(Received 28 March 2012; accepted 6 June 2012; published online 2 July 2012)

The effect of quantum mechanics (QM) on the details of the nucleation process is explored employing Ne clusters as test cases due to their semi-quantal nature. In particular, we investigate the impact of quantum mechanics on both condensation and dissociation rates in the framework of the microcanonical ensemble. Using both classical trajectories and two semi-quantal approaches (zero point averaged dynamics, ZPAD, and Gaussian-based time dependent Hartree, G-TDH) to model cluster and collision dynamics, we simulate the dissociation and monomer capture for Ne_8 as a function of the cluster internal energy, impact parameter and collision speed. The results for the capture probability $P_s(b)$ as a function of the impact parameter suggest that classical trajectories always underestimate capture probabilities with respect to ZPAD, albeit at most by 15%–20% in the cases we studied. They also do so in some important situations when using G-TDH. More interestingly, dissociation rates k_{diss} are grossly overestimated by classical mechanics, at least by one order of magnitude. We interpret both behaviours as mainly due to the reduced amount of kinetic energy available to a quantum cluster for a chosen total internal energy. We also find that the decrease in monomer dissociation energy due to zero point energy effects plays a key role in defining dissociation rates. In fact, semi-quantal and classical results for k_{diss} seem to follow a common "corresponding states" behaviour when the proper definition of internal and dissociation energies are used in a transition state model estimation of the evaporation rate constants. © *2012 American Institute of Physics*. [http://dx.doi.org/10.1063/1.4730033]

I. INTRODUCTION

The formation of a new condensed phase, whether solid from liquid (e.g., crystallization), liquid from vapor (e.g., dew formation), or simply the segregation of a component as in micelle formation is a widespread process in nature. Controlling such processes appears to be of paramount importance especially in technologically or environmentally relevant contexts; in fact, it may lead to near defect-free crystals (e.g., in silicon or GaAs), improved conduction properties (e.g., in carbon nanotube-doped polymeric materials[1]) or controlled nanoparticle sizes (e.g., in the vapor synthesis of metal clusters[2]).

Even the somewhat simple cases of crystal formation from a molten species, for which classical nucleation theory (CNT) (Refs. 3–6) could be expected to work reasonably well due to the dense nature of the system, do not cease to amaze.[7] Albeit not complicated by polymorphism in the high density phase, the process of liquid nucleation from vapor is also not as clear as one would like it to be with respect to molecular level details and time scales. For instance, model calculations[8] as well as large scale simulations[9–12] have provided evidence that CNT presents serious shortcomings even for simple systems such as rare gases. The reason for these shortcomings may be manifold: an incorrect estimate of the free energy of small clusters,[13] the incorrect assumption of cluster sphericity,[12,14] the capillary approximation,[15] or the assumption of a well-defined system temperature. This last assumption might be violated due to a poor separation of time scales between monomer capture by a metastable cluster M_n and the thermalization of the resulting species. This could appear to be of minor importance since it is likely to play a substantial role only in the case of clusters with limited size (i.e., small n) and only for macroscopically short timespans after the system has reached supersaturation. However, critical clusters (i.e., the ones for which growing or shrinking in size have comparable rates) may be quite small ($\sim 10 \leq n \leq 200$), and growth can be inhibited by a sudden dilution which happens during a free expansion through a nozzle. Hence, studying the key steps (capture, dissociation, and collisional energy transfer) of the nucleation process in the microcanonical framework may help addressing the concern of the validity of the constant temperature hypothesis.

Several groups have indeed conducted detailed numerical investigations on two key dynamical steps in the nucleation process, namely, monomer capture[16–19] and dissociation[21–23] from a metastable cluster M_n using microcanonical approaches. In all cases, classical dynamics simulations were used to study the dynamical features of the two processes, thus disregarding the possible impact of quantum mechanics (QM). In fairness, many of the systems studied previously

a)On leave from School of Chemistry, Cardiff University, Main Building, Park Place, Cardiff CF10 3AT, United Kingdom. Electronic addresses: Massimo.Mella@uninsubria.it and MellaM@cardiff.ac.uk.

 © 2012 American Institute of Physics

Downloaded 02 Jul 2012 to 193.205.162.64. Redistribution subject to AIP license or copyright; see http://jcp.aip.org/about/rights_and_permissions

should not be expected to present strong quantum mechanical effects due to a large monomer mass and weak interaction between monomers (e.g., Ar).[16,17,21,22,40] This, however, cannot be considered as a general rule. For instance, Al_n (Ref. 23) exhibits an important amount of zero point energy. Also, experiments have suggested that quantum effects should be important in the free evaporation from H_2O/D_2O mixtures[24] where H_2O escapes the condensed phase faster. Hence, the experiments in Ref. 24 indicate that QM have some impact on the relative rates of isotopically substituted compounds. It is reasonable to expect that quantum effects should also play a role in modifying the absolute quantitative value of condensation and evaporation rates with respect to a classical mechanics description. Support to this idea is provided by the simple observation that D_2O should be more classical (smaller rotational constants and vibrational frequencies) than normal water due to isotopic substitution. This was evidenced in recent simulation results showing a higher C_p for D_2O than for H_2O.[25] The lower zero point libration energy and the higher density of states for D_2O (Ref. 26) have an impact on dissociation energies and on the amount of energy exchange, which obviously bears importance for the nucleation process.

In order to provide more quantitative indications on the role played by quantum effects during nucleation, we have investigated both dissociation and capture of Ne atoms from and by Ne_n clusters. The rationale for this choice is multifaceted. Ne clusters are expected to be sufficiently quantum in nature to show clear-cut effects in the quantitative details of the studied processes. Nevertheless, their quantum effects are not so strong as to invalidate the use of a semi-quantal approach, since the de Boer parameter is roughly $\Lambda \simeq 0.58$. In addition, accurate pair potentials for Ne are available. Moreover, the atomic nature of the monomer represents a substantial simplification for theory. Also, the isotropic nature of the interaction between Ne atoms implies that quantum effects play a role only because of hindered translational modes (i.e., vibrations). Conversely, water, or its isotopomers, would exhibit effects deriving from hindered rotations (or librations) as well, a fact that complicates the emerging picture.

The organization of the paper is as follows. In Sec. II, we discuss our methodology and computational techniques for addressing the role played by quantum mechanics in the chemical physics of Ne clusters. Section III provides one with our quantitative results and their analysis. Finally, Sec. IV gives the final discussion and conclusion, setting the stage for future work.

II. THEORY

Atomic units (i.e., bohr) will be assumed throughout the manuscript for distances; energies are given in cm^{-1}. Finally, velocities are expressed in bohr ps^{-1}.

To investigate the possible effects due to quantum mechanics in two fundamental steps of the nucleation process, namely, monomer capture and dissociation, several approaches were employed. We used diffusion Monte Carlo[27] to compute the ground state energy and anharmonic zero point energy (aZPE) for several cluster sizes. These data are useful to provide estimates for monomer association and dissociation energy, as well as to set a lower bound for the internal energy of the cluster sizes investigated. Comparing with similar estimates obtained using the harmonic approximation for the ZPE (hZPE), it is also possible to measure quantitatively the effect of anharmonicity (or "floppiness") of these species. The time-dependent evolution was described using three different approaches, namely, classical trajectories (CT), the zero point averaged dynamics (ZPAD),[28,29] and the semi-quantum Gaussian-based time dependent Hartree (G-TDH) method.[30] In the following, a brief account of all the methods employed is given in order to make the discussion of our results self-contained.

A. Diffusion Monte Carlo

Diffusion Monte Carlo (DMC) allows one to sample a distribution of configurations $\{\mathbf{R}_i\}$, with $\mathbf{R} = (\mathbf{r}_1, \ldots, \mathbf{r}_j, \ldots, \mathbf{r}_n)$ being a vector giving the position of n distinguishable or bosonic particles in a 3D Cartesian space, distributed accordingly to the ground state wave function ϕ_0 of the Hamiltonian

$$\mathcal{H} = -\frac{1}{2}\sum_{j=1}^{n}\frac{\nabla_j^2}{m_j} + V(\mathbf{R}). \tag{1}$$

It relies on the possibility of writing a short-time step (δt) approximation to Green's function $\langle \mathbf{R}'|e^{-t\mathcal{H}}|\mathbf{R}\rangle = G(\mathbf{R} \rightarrow \mathbf{R}', t)$ of the imaginary-time Schrödinger equation associated to the operator in Eq. (1). In particular, it is important to assess that a particular approximation to Green's function is associated with a well-defined order m of the discretization error $\mathcal{O}(\delta t^m)$, in order to ensure robust and accurate results that can either be extrapolated *a posteriori* to $\delta t \rightarrow 0$,[32] or "on the fly" as recently proposed.[33]

For systems presenting only a partial quantum nature and sufficiently bound such as Ne clusters, the simplest version of DMC without importance sampling (noIS-DMC) (Ref. 34) can be employed provided that a sufficiently large population N of configurations (walkers or psips) is used in the sampling process and the "step to step" stochastic error is minimized.[35] In this work we opted for the third-order "on the fly" propagator implemented in Ref. 33. It is based on a two-step procedure that allows the extrapolation of second-order branching weights to third-order ones. For all simulations a time step $\delta t = 100$ a.u. was used, which guarantees a time step bias of the order of the statistical error associated with our results even in the case of the simplest second-order Trotter factorization tested previously.[34] In order to reduce the bias due to population error, we linearly extrapolated two calculations ($N = 4000$ and 8000) with respect to $1/N$.[36]

As often done for weakly interacting atoms such as rare gases, the total potential is written as

$$V(\mathbf{R}) = \sum_{j<k=1}^{n} u(r_{jk}), \tag{2}$$

where the pair interaction potential is the one proposed by Aziz and Slaman.[37] To facilitate a few technical steps in the implementation of the dynamical methods described in the following, $u(r_{jk})$ was fitted with a linear combination of

Downloaded 02 Jul 2012 to 193.205.162.64. Redistribution subject to AIP license or copyright; see http://jcp.aip.org/about/rights_and_permissions

10 Gaussian functions centered at zero distance. The global fit is fairly accurate, with a maximum error in the range of 10^{-6}. The minimum of the potential has a well depth of 29.36 cm^{-1} at 5.84 bohrs. A mass of 36 443.99 atomic units was used for Ne in all calculations.

B. Classical trajectory simulations

To simulate both monomer dissociation and capture, classical dynamics trajectories represent the most convenient and cost-effective approach. This method has been used previously in many studies on these topics,[18,22,23,38,39,41] and it has inspired several conceptual models useful for predicting the dependency of the quantitative results on system parameters. In all classical simulations, we employed the same protocols followed by one of us in previous investigations;[16,21] therefore, we give only a few details in the following.

In short, cluster dissociation at a specific total energy E (in the center of mass reference frame) was studied after an initial equilibration stage conducted by means of a Metropolis Monte Carlo (MMC) simulation in the microcanonical ensemble.[42] During the MMC runs, each of the atoms in the cluster was constrained to have its distance from the center of mass of the remaining ones shorter than 20 bohrs. Trajectories were started from statistically independent samples extracted from the MMC simulations; 2000–5000 total trajectories per (n, E) pair were run for $n = 8$, 13, 14, 19. Trajectories were integrated using the leap frog algorithm and a time step of 200 a.u. (roughly 5 fs) up to a maximum of 120 ps. The total energy was conserved better than 10 ppm in all cases. Initial velocities for all particles were chosen according to the stochastic procedure suggested in Ref. 43. The dissociation rates were determined as follows. The time evolution of $\ln[(N_0 - N_\tau)/N_0]$ was fitted with $-k\tau$, N_τ being the number of dissociated trajectories at time τ. A trajectory was dubbed as "dissociated" whenever a cluster atom was found at a distance larger than 20 bohrs from the center of mass (CoM) of the remaining cluster. This procedure assumes that the decay can be described by a single exponential. If this were not the case, the value of k would represent a lower bound to the statistical dissociation rate, which is given by the short time fit.[23] However, deviation from single exponential behaviour was found to be limited in the explored range. We thus only quote the values obtained with the global fits. Notice that the total angular momentum J of the Ne_n cluster is not specified (i.e., we are working in the microcanonical ensemble without J resolution): according to the results in Ref. 21, it bears negligible importance on the quantitative results for rare gas clusters in the range of angular momentum values that is likely to be populated in the NVE ensemble.

Capture (or sticking) $P_s(n, b, E, v_p)$ probabilities of a monomer by a Ne_n cluster are defined as the fraction of trajectories (N_s/N_0) that led to a monomer-cluster capture for a chosen set of ensemble conditions (i.e., n, impact parameter b, E, and projectile-target relative speed v_p). The initial condition for the target clusters was generated in the same way as for the dissociation simulations; the projectile was placed at a distance of at least 40 bohrs from the CoM of the target in order to have negligible interaction with the latter. A capture event was deemed as happened after a collision when the projection of the relative projectile-cluster velocity v_p along the vector joining the CoM of the two species changed sign a chosen number of times N_{tp}. As before,[16] we found $P_s(n, b, E, v_p)$ to be very weakly dependent on N_{tp} if $N_{tp} \geq 3$ and on the angular momentum J of the cluster; thus, $N_{tp} = 5$ was employed as a convenient definition and no selection was made on the absolute value of J.

C. Zero point averaged dynamics

The ZPAD method, originally introduced to study dynamical processes in Ne and He droplets,[28,29] hinges on the idea that it may be possible to describe the dynamical processes of a quantum atomic cluster by associating each atom with a single particle wave function, which replaces the point particle with a symmetric probability distribution function, and accounts, at least partially, for quantum effects such as ZPE and a longer average interatomic distance than predicted from the minimum of the pair potential. Once defined, the wave function $\phi(\mathbf{r})$ moves with the atom, but it is otherwise unchanged by the dynamics. As a result, the application of the Ehrenfest theorem gives equations of motion that are the same ones as for classical dynamics but on an effective potential. The latter is the original pair potential averaged over the atomic wave functions. Clearly, such an approach is appropriate if $\phi(\mathbf{r})$ is sufficiently compact, i.e., if quantum effects on the dynamics are not overwhelming. This seems to be the case even for quantum systems such as solid hydrogen, for which a similar approach has encountered a good degree of success.[44,45]

To avoid exploiting experimental information in defining the features of $\phi(\mathbf{r})$, the ZPAD approach employs a self-consistent iterative procedure based on an alternation between classical simulations on effective potentials and quantum calculations to optimize the atomic wave function $\phi(\mathbf{r})$. Since the original ZPAD method was derived for a constant temperature system while we work in the microcanonical ensemble, a few details of the optimization procedure described in Ref. 28 had to be modified accordingly. In particular, the classical simulations employed to build the inter-particle radial distribution functions needed to define the caging potential experienced by each atom must be run with a constant energy method. For convenience, we employed the same MMC approach used for the classical simulations, albeit constant energy classical trajectories would have worked as well. Also, we selected a spherical Gaussian function $\mathcal{N}_\alpha e^{-\alpha(\mathbf{r}-\mathbf{r}_{class})^2}$ as a trial form for $\phi(\mathbf{r})$ in order to maintain simplicity and optimized its width α by minimizing the average energy of a Ne atom inside the caging potential; in previous applications, the shape of $\phi(\mathbf{r})$ was obtained by solving numerically the Schrödinger equation. Assuming a Gaussian form for $\phi(\mathbf{r})$ centered on the atom center of mass $\mathbf{r}_{class}$ facilitates the calculation of the effective potential, leaving unchanged its sum of Gaussians form. To avoid starting MMC simulations from a cluster geometry with a potential energy higher than the assigned cluster total energy, we found useful to begin those simulations from a locally minimized structure after every update of $\phi(\mathbf{r})$ and the effective pair potential.

Downloaded 02 Jul 2012 to 193.205.162.64. Redistribution subject to AIP license or copyright; see http://jcp.aip.org/about/rights_and_permissions

In conclusion, the ZPAD approach allows one to define an effective pair potential $u_{eff}(r_{jk})$ and associated particle wave functions for any specific value of E. As shown in the following, this effective potential exhibits a reduced well depth representing the fact that part of the internal energy is "frozen" into ZPE. Also, its equilibrium distance is found to be longer than the classical one. Note that $u_{eff}(r_{jk})$ is, in principle, state and size dependent and it should be updated "on the fly" after any changes that alter either n or E. Whether this is indeed necessary ought to be investigated on a case by case basis.

D. Gaussian-based time dependent Hartree (G-TDH) dynamics

As hinted in Sec. II C, a possible shortcoming of the ZPAD dynamics is related to its inability to cope with a change in the energy content and composition of a system since it requires an *a priori* definition of the effective potential over which the dynamics takes place. In the formulation presented above, adapting to a new state would be equivalent to allowing the width of the Gaussian $\phi(\mathbf{r})$ to adjust dynamically during the system evolution, a task that requires a set of equations coupling atomic positions and momenta with α. This can be achieved, again, assuming that the wave function for the system can be written as a product of Gaussian terms[30]

$$|\Psi(\mathbf{R},t)\rangle = a(t)\prod_{j=1}^{n}|\chi_j(\mathbf{r}_j,t)\rangle, \tag{3}$$

with

$$|\chi_j(\mathbf{r}_j,t)\rangle = \left(\frac{2\alpha_j(t)}{\pi}\right)^{3/4}\exp[-\gamma_j(t)(\mathbf{r}_j-\mathbf{r}_{0j}(t))^2 + i\mathbf{p}_{0j}(t)(\mathbf{r}_j-\mathbf{r}_{0j}(t))], \tag{4}$$

for every particle. From this ansatz and the Dirac–Frenkel variational principle,[46,47] it is possible to derive a set of equations of motion that propagate the average atomic positions $\mathbf{r}_{0j}(t)$, momenta $\mathbf{p}_{0j}(t)$, phase $a(t)$, and complex width $\gamma_j(t) = \alpha_j(t) + i\beta_j(t)$. Here, $\alpha_j(t)$ and $\beta_j(t)$ are the real and imaginary part of $\gamma_j(t)$ (note that $\alpha_j > 0$). The resulting equations for each atom in the system are

$$\dot{\alpha}_j = 4\alpha_j\beta_j\left[\frac{1}{m_j}-\frac{1}{M}\right], \tag{5}$$

$$\dot{\beta}_j = -2\left(\alpha_j^2-\beta_j^2\right)\left[\frac{1}{m_j}-\frac{1}{M}\right]-\frac{8}{3}\alpha_j^2V^{(\alpha_j,0)}, \tag{6}$$

$$\dot{\mathbf{r}}_{0j} = \frac{\mathbf{p}_{0j}}{m_j}-\frac{\mathbf{P}}{M}, \tag{7}$$

$$\dot{\mathbf{p}}_{0j} = -\nabla_{\mathbf{r}_j}V, \tag{8}$$

where $V = \langle\Psi(\mathbf{R},t)|V(\mathbf{R})|\Psi(\mathbf{R},t)\rangle$, $V^{(\alpha_j,0)} = \langle\frac{\partial\Psi(\mathbf{R},t)}{\partial\alpha_j}|V(\mathbf{R})|\Psi(\mathbf{R},t)\rangle = -\frac{1}{16\alpha_j^2}\langle\Psi(\mathbf{R},t)|\frac{\partial^2V(\mathbf{R})}{\partial\mathbf{r}_{0j}^2}|\Psi(\mathbf{R},t)\rangle$, $\mathbf{P}$ being the total momentum of the system and M its total mass. Notice that, thanks to the analytical form of the pair potential, the integrals needed in the propagation of the wave function are computed analytically, and that the number of degrees of freedom is larger by a factor of two with respect to a classical simulation. Thus, the computational cost of G-TDH scales identically to the one of molecular dynamics. The equations are integrated with a 4th order Runge-Kutta algorithm with a time step of 10 atomic units (i.e., $\simeq$0.24 fs, compared with $\simeq$5 fs for classical trajectories). As an indication, it is mentioned that the computational time to calculate one point in the capture probability curve with 2000 trajectories is about 1 h on 12 Xeon 5650 cores.

Equations (5)–(8) can be solved simultaneously for all atoms, with the initial conditions obtained as follows. For the clusters, $\mathbf{r}_{0j}(t=0)$ and $\gamma_j(t=0)[=\alpha_j(t=0)]$ correspond to the minimum energy configuration obtained by imaginary time propagation, as detailed below. Subsequently, the $\mathbf{p}_{0j}(t=0)$ is chosen randomly following a normal distribution over all degrees of freedom in order to obtain the chosen total energy of the cluster. Given the usually fast intramolecular vibrational redistribution (IVR) afforded by rare gas clusters, this procedure is not expected to introduce any important bias into the cluster dissociation rate provided that the average lifetime is longer than the IVR decay time (roughly 30 ps (Ref. 20)).

For the collision studies, the initial projectile position and momentum are chosen according to the given impact parameter and collision energy. It was placed at a distance of 80 bohrs from the CoM of the cluster to ensure cluster thermalization (i.e., that the kinetic energy is statistically redistributed among the degrees of freedom) before collision. To avoid a spread of the free particle wave packet, the width of the projectile was maintained frozen ($\beta_{proj}=0$) until the dispersing term in Eq. (6) from kinetic origin became smaller than a fraction q of the focusing term coming from the potential, i.e.

$$\left|2(\alpha_{proj}^2-\beta_{proj}^2)\left[\frac{1}{m_{proj}}-\frac{1}{M}\right]\right| < q\left|\frac{8}{3}\alpha^2V_{proj}^{(\alpha,0)}\right| \tag{9}$$

with q chosen so that less than 10% of the trajectories do not reach this threshold. We found that there is a range of values ($0.375 \le \alpha \le 1.5$) for which the capture probabilities are the same (*vide infra*, bottom panel of Fig. 7). Thus, $\alpha = 1.5$ is used in the following. Note that in a full quantum approach, the spread of the projectile wave packet does not pose any special problem since it is a superposition of several free particle energy states, with the result of a collision analyzed as a function of energy. In our case, however, we defined the energy and impact parameter of the collision by the corresponding expectation values of the Gaussian wave packet. Therefore, it would make no sense to analyze the energy content in the outgoing wave packet since the method constrains the wave packet to remain Gaussian at all times.

As stated above, the initial positions and width parameters for the cluster atoms are obtained by the imaginary time propagation. This method consists in solving the time-dependent Schrödinger equation in which time is replaced by an imaginary variable, thus resulting in an energy minimization as a function of the parameters describing the high-dimensional wave function. The corresponding

Downloaded 02 Jul 2012 to 193.205.162.64. Redistribution subject to AIP license or copyright; see http://jcp.aip.org/about/rights_and_permissions

TABLE I. Global minimum potential (V_{min}), ground state energy obtained using DMC simulations ($E_0^{DMC}(n)$), the harmonic approximation ($E_0^{HA}(n)$), and the G-TDH model ($E_0^{G\text{-}TDH}(n)$) for Ne_n species, in cm^{-1}. The energy difference $\Delta_0(n)$ for the $Ne_n \rightarrow Ne_{n-1}$ + Ne process is shown in a few selected cases as obtained from the DMC, HA, and G-TDH results. (See Fig. 1 for energy definitions.)

n	V_{min}	$E_0^{DMC}(n)$	Δ_0^{DMC}	DMC ZPE	$E_0^{HA}(n)$	Δ_0^{HA}	$E_0^{G\text{-}TDH}(n)$	$\Delta_0^{G\text{-}TDH}$
5	− 263.809	− 156.771(4)		106.533(4)	− 140.903		− 126.637	
7	− 474.504	− 288.17(4)		186.334(4)	− 262.053		− 250.201	
8	− 569.317	− 346.77(8)	58.60(9)	221.65(8)	− 316.043	65.842	− 305.070	54.8687
12	− 1078.5	− 682.7(1)		402.5(1)	− 638.671		− 625.503	
13	− 1258.25	− 801.5(2)	118.7(2)	456.1(2)	− 754.993	129.49	− 746.214	120.711
14	− 1356.57	− 866.3(2)	64.8(3)	489.7(2)	− 814.251	59.2582	− 803.277	57.0634
18	− 1870.58	− 1208.2(3)		662.2(3)	− 1145.44		− 1132.490	
19	− 2048.14	− 1329.6(2)	118.5(3)	721.6(2)	− 1266.37	120.711	− 1248.810	116.322

equations are

$$\dot{\alpha}_j = -\left\{2\left(\alpha_j^2 - \beta_j^2\right)\left[\frac{1}{m_j} - \frac{1}{M}\right] + \frac{8}{3}\alpha_j^2 V^{(\alpha_{\mathbf{r}_j},0)}\right\}, \quad (10)$$

$$\dot{\beta}_j = -4\alpha_j\beta_j\left[\frac{1}{m_j} - \frac{1}{M}\right], \quad (11)$$

$$\dot{\mathbf{r}}_{0j} = \frac{\beta_j}{\alpha_j}\left(\frac{\mathbf{p}_{0j}}{m_j} - \frac{\mathbf{P}}{M}\right) + \frac{1}{2\alpha_j}\nabla_{\mathbf{r}_j} V, \quad (12)$$

$$\dot{\mathbf{p}}_{0j} = -\frac{2|\gamma|_j^2}{\alpha_j}\left[\left(\frac{\mathbf{p}_{0j}}{m_j} - \frac{\mathbf{P}}{M}\right) + \frac{\beta_j}{2|\gamma|_j^2}\nabla_{\mathbf{r}_j} V\right]. \quad (13)$$

The initial conditions for imaginary time propagation are taken from the Cambridge Cluster Database[48] Ar_n structure, appropriately rescaled, and α_j initial value is chosen as the width of the best Gaussian approximation for the vibrational ground state of Ne_2. Notice that the parameter β_j goes to zero whatever its initial value according to Eq. (11), so it is set to zero.

The clear advantage of G-TDH with respect to the ZPAD method discussed above is its ability to adjust the wave function, at least in a mean field sense, to the current situation of the system. In this respect, our model wave function for the Ne_n systems describes each atom in the cluster with an independently optimized or propagated Gaussian width. In principle, this permits to tailor the atomic description to the different local environment (e.g., in the core of the cluster or on its surface), thus allowing to account for a different "pressure" or caging exerted by the nearest neighbours. At this stage, we would expect the chosen model (Eqs. (3) and (4)) to guarantee reasonably accurate results since it implicitly contains terms depending on inter-particle distances (also, *vide infra* Table I for a quantitative comparison); this can be evidenced by re-expressing the product between the Gaussians centered on two different atoms in terms of their relative distance vector and center of mass position using the Gaussian multiplication theorem.

III. RESULTS

In the following we shall discuss the results obtained for monomer capture and dissociation of Ne_8, for which we employed all the approaches discussed in Sec. II to investigate the effects due to quantum behaviour. Results for larger clusters obtained using classical dynamics and ZPAD on Ne_n ($n = 13$, 14, 19) can be found in the supplementary material[31] and are referred to only if needed.

To facilitate the comparison between results and the ensuing discussion, Fig. 1 provides a graphical definition for all the energetic quantities employed in this work. Notice that our energy zero is taken as the situation of infinite separation and complete rest for all the Ne atoms.

A. DMC results

The results of the DMC simulations on Ne_n for $n = 5$, 7, 8, 13, 14, 18, and 19 are shown in Table I. Classical minimum potential energy structures are shown in Fig. 2. These clusters were chosen to be as representative as possible of the size-dependent features that can be presented by Ne_n. In particular $n = 13$ and 19 represent closed-shell or magic number clusters, whereas Ne_{14} is archetypical for species with adatoms. Ne_8 was chosen for its partial fluxional nature. Some of the studied clusters (e.g., $n = 7$, 13, and 18) were included to provide statistically exact dissociation energies as references for

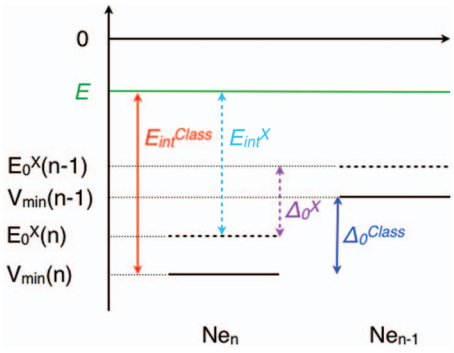

FIG. 1. Definition of various energetic quantities used in the main text. The energy zero is taken as the situation of infinite separation and complete rest for all the Ne atoms. X stands for classical, ZPAD, or G-TDH simulation method. $V_{min}(n)$ is the minimum of the Ne_n potential energy, and $E_0^X(n)$ is the energy of the Ne_n ground state level for method X. Note that $E_0^{Class}(n) = V_{min}(n)$. Δ_0^X is defined as the binding energy of the nth Ne atom for method X, i.e., $\Delta_0^X = E_0^X(n-1) - E_0^X(n)$. E is the total energy of the system in the center of mass reference frame, and E_{int}^X the corresponding internal energy for method X, i.e., $E_{int}^X = E - E_0^X(n)$.

Downloaded 02 Jul 2012 to 193.205.162.64. Redistribution subject to AIP license or copyright; see http://jcp.aip.org/about/rights_and_permissions

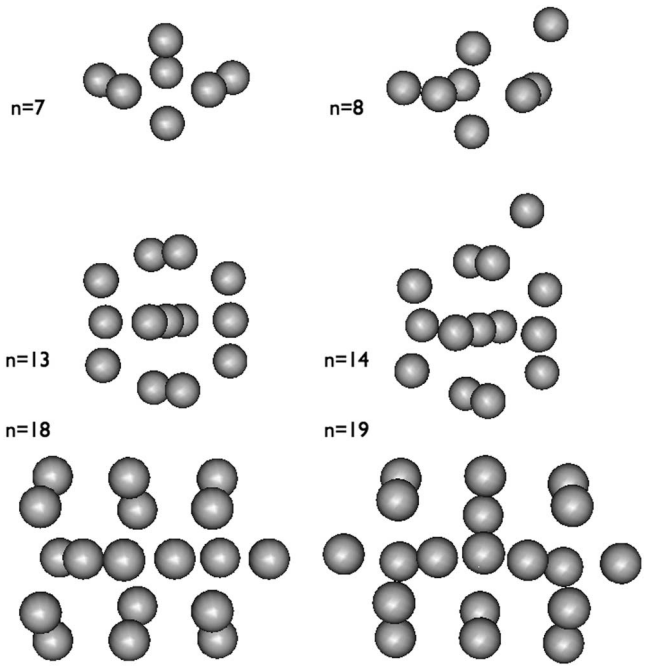

FIG. 2. Global minimum geometries for Ne_n ($n = 7$, 8, 13, 14, 18, 19) on the classical pair potential surface.

the dynamical simulations. Table I also provides the results for the ground state energy of these clusters computed with the harmonic approximation or the G-TDH model. The clusters studied in this work maintain their classical global minimum shape when ZPE effects are taken into account using either the harmonic approximation or the G-TDH model to approximate the ground state. In the latter case, the interatomic equilibrium distances are slightly longer than in the classical minima shown in Fig. 2. For reference, also the potential energy of the global minimum for each species is given.

As expected, Table I shows that the DMC ground state energies are lower than the ones provided by the harmonic approximation (HA) and G-TDH, with the value for the latter being only slightly higher than for the HA. This shows the good performance of the model wave function employed in G-TDH in describing Ne_n clusters.

A closer inspection of the energy differences between DMC and HA or G-TDH shows that anharmonic effects do not play a key role for the Ne_n studied in this work. However, slightly larger differences are seen for a cluster such as Ne_7 that has nearly degenerate low energy minima.[34] Quantitatively, the ZPE reduces by roughly 30% the total binding energy for a cluster (i.e., the energy difference for the reaction $Ne_n \rightarrow n$Ne), and as such it represents a substantial contribution to the energetics of any transformation involving these species. As an example, Ne_{14} is predicted by DMC to require roughly 66 cm^{-1} to dissociate an atom. However, the classical dissociation energy, given by the potential energy difference, is 98 cm^{-1}, i.e., roughly 50% larger. Both the HA and G-TDH methods provide estimates close to the DMC ones. The impact of quantum effects is actually expected to be stronger than a simple reduction of the dissociation barrier, since the non-availability of the ZPE for the dynamical processes reduces the amount of energy that can flow into the reactive modes for a given value of the total energy (see Sec. IV).

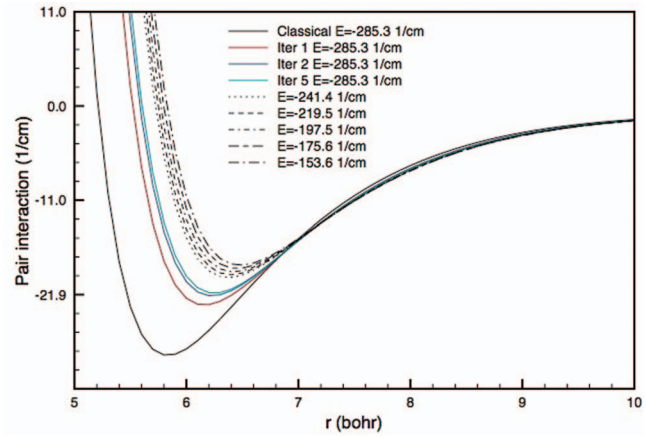

FIG. 3. Classical and effective $u_{eff}(r_{jk})$ pair potentials for Ne_8 as a function of the total cluster energy. For $E = -285.3$ cm^{-1}, $u_{eff}(r_{jk})$ is also shown for selected iteration numbers.

B. Dissociation rates

1. ZPAD effective potentials

The first step in the ZPAD dynamical simulations is the determination of the (state-dependent) effective potential $u_{eff}(r_{jk})$ (see Sec. II C). In practice, we employed MMC simulations to generate at least 50 millions of statistically independent samples for the structure of a cluster at each chosen energy. This allowed us to generate precise inter-particle distributions. The converged results for $u_{eff}(r_{jk})$ at several energies for Ne_8 are shown in Fig. 3, together with the results for selected iteration steps at $E = 285.3$ cm^{-1}, the lowest energy at which we ran the ZPAD simulations. As can be seen, $u_{eff}(r_{jk})$ requires only a few iterations to converge (usually 4–5 iterations) and only minor fluctuations are evidenced at a close scrutiny, thanks to the large statistical sample used to compute the inter-particle distributions. Also, the state-dependent nature of $u_{eff}(r_{jk})$ emerges clearly from the fact that the bottom of the well rises and the equilibrium distance increases upon increasing the total energy of the clusters. Bearing in mind that higher energy usually implies wider structural fluctuations, we consider this feature a clear expression of the larger ensemble of states made available to our systems by shallower wells. These structural and energetic changes upon increasing the internal energy are also paralleled by an increase in the width of the Gaussian "dressing" each Ne atom, which is interpreted as an indication that the atomic particles become less localized following an increase of E. However, the $u_{eff}(r_{jk})$ well depth appears to depend only weakly on E; in fact, the well depth changes by at most 15% upon increasing the internal energy by roughly 50%. Similarly, the pair equilibrium distance increases by roughly 6% over the same energy interval. Such weak dependency on E will be used in the following to interpret the numerical results for both k_{diss} and P_s.

Downloaded 02 Jul 2012 to 193.205.162.64. Redistribution subject to AIP license or copyright; see http://jcp.aip.org/about/rights_and_permissions

TABLE II. Dissociation rate k_{diss} for Ne_8 as a function of the total energy of the cluster E as computed using classical, ZPAD, and G-TDH simulations. Also shown is the dissociation energy Δ_0^{ZPAD} for the process $Ne_n \rightarrow Ne_{n-1}$ + Ne as a function of E when both Ne_8 and Ne_7 are described by the effective potential $u_{eff}(r_{jk})$ specifically optimized for Ne_8 at its chosen energy. Energies in cm^{-1} and rates in ps^{-1}. For the classical simulations, $\Delta_0 = 93.71\ cm^{-1}$.

E	k_{diss}^{Class}	k_{diss}^{ZPAD}	$k_{diss}^{G\text{-}TDH}$	Δ_0^{ZPAD}
−374.424	0.0000559765			
−329.212	0.000924297			
−285.317	0.00496395	0.00001		65.6229
−241.422	0.0173174	0.000173469		64.0866
−219.475	0.024344	0.000819547		62.9892
−197.527	0.0374608	0.00304012		61.8918
−175.58		0.00593788	0.00012	60.7945
−153.632		0.0112638	0.00074	60.3555
−131.685		0.0257542	0.0046	59.9166
−109.737			0.010	
−87.7899			0.015	
−65.8424			0.056	

2. Ne_8 dissociation rates

Table II provides the microcanonical dissociation rates of Ne_8 obtained with the classical trajectories, ZPAD, and G-TDH methods as a function of the total energy E, and the top panel of Fig. 4 provides a pictorial view of the results. The ZPAD and G-TDH methods clearly provide much lower values than the classical ones. This is a consequence of quantum effects. In ZPAD they translate into a lower well depth, and in G-TDH they result in a large amount of the classical internal energy being locked into zero-point motion. In other words, for a given value of the total energy, the species described with ZPAD and G-TDH have a lower amount of rotational and vibrational energy to inject into the dynamics along the reaction coordinate. Thus, it becomes less likely for an atom to gather enough kinetic energy to escape the cluster, despite the fact that the dissociation threshold is also lowered (see the DMC and G-TDH results in Table I).

The effect due to barrier reduction or to changes in the phase space volume between the three methods can be highlighted by comparing dissociation rates obtained with the same amount of *available* internal energy (E_{int}^X, defined in Fig. 1 which depends on the method). The bottom panel in Fig. 4 shows the same Ne_8 dissociation rates as in the top panel, but this time as a function of E_{int}^X, $X \equiv$ classical, ZPAD, or G-TDH. Surprisingly, the classical dissociation is slower by two orders of magnitude than the other two, while G-TDH and ZPAD differ only by roughly 50%.

3. Rice–Ramsberger-Kassel (RRK) analysis of Ne_8 dissociation rates

The top panel of Fig. 5 shows a log-log plot of the dissociation rates against $\frac{E_{int}-\Delta_0^{Class}}{E_{int}}$, with $E_{int} - \Delta_0^{Class}$ being the maximum internal energy available to the daughter cluster Ne_7 (see Fig. 1). As found previously for these systems,[21] the classical dissociation rates closely follow an RKR behaviour (i.e., $k_{diss} \propto (\frac{E_{int}-\Delta_0^{Class}}{E_{int}})^{s-1}$). This seems to be also the case

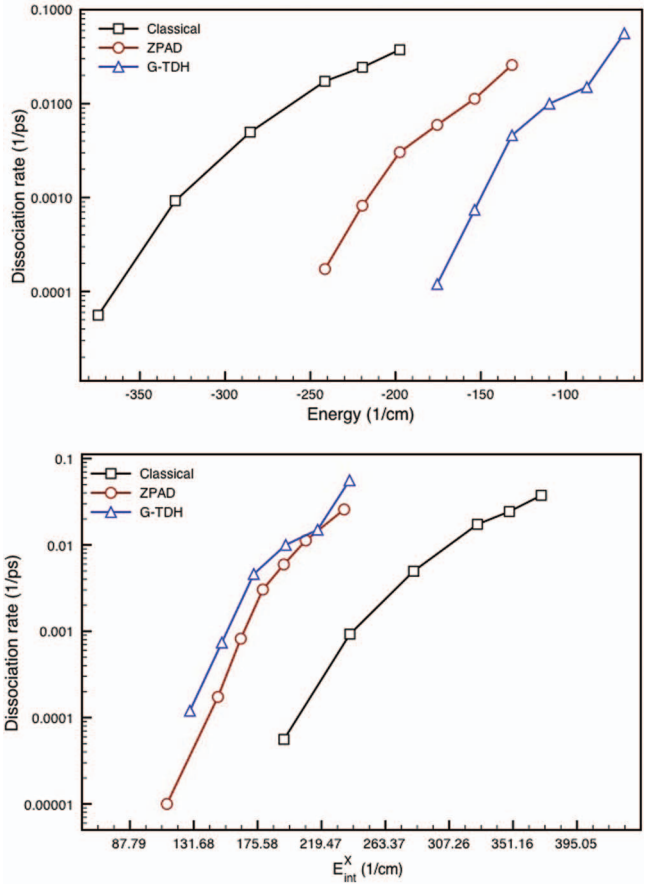

FIG. 4. Top panel: Ne_8 dissociation rates k_{diss} (log scale) versus total energy E. Bottom panel: Same dissociation rates shown as a function of E_{int}^X, the internal energy of Ne_8 in each method. Rates in ps^{-1}, energies in cm^{-1}.

for the ZPAD and the G-TDH rates, albeit the slope (hence s) seems to be higher than in the classical case. A change in slope is readily apparent at $Log(\frac{E_{kin}-\Delta_0^{Class}}{E_{kin}}) \sim -0.1$ in the G-TDH rates. A closer inspection shows a similar feature for the classical trajectories and ZPAD dynamics, even though it seems less marked.

Such a characteristic is often attributed to the transformation of a rare gas cluster from solid-like to liquid-like,[21] and it is reminiscent of the "back bending" often witnessed in its caloric curve.[49] This phenomenon is responsible for a reduction of the average kinetic energy available to the atoms upon transition to a less compact, thus more energetic, structure or structural ensemble when its microcanonical energy is increased.

The relative behaviour of ZPAD and G-TDH with respect to classical k_{diss} shown in the bottom panel of Fig. 4 suggests that an important role is played by the different dissociation energy afforded by each method. Hence in the bottom plot of Fig. 5 we compare the k_{diss} results as function of $\frac{E_{int}^X-\Delta_0^X}{E_{int}^X}$, where $E_{int}^X - \Delta_0^X$ is the maximum internal energy available to the daughter cluster Ne_7 in each method (see Fig. 1). (Note that Δ_0^{ZPAD} was calculated using $u_{eff}(r_{jk})$ of the parent cluster.)[50] Compared to the top panel, the ZPAD and G-TDH rate constants are shifted to the left and show a smaller slope,

Downloaded 02 Jul 2012 to 193.205.162.64. Redistribution subject to AIP license or copyright; see http://jcp.aip.org/about/rights_and_permissions

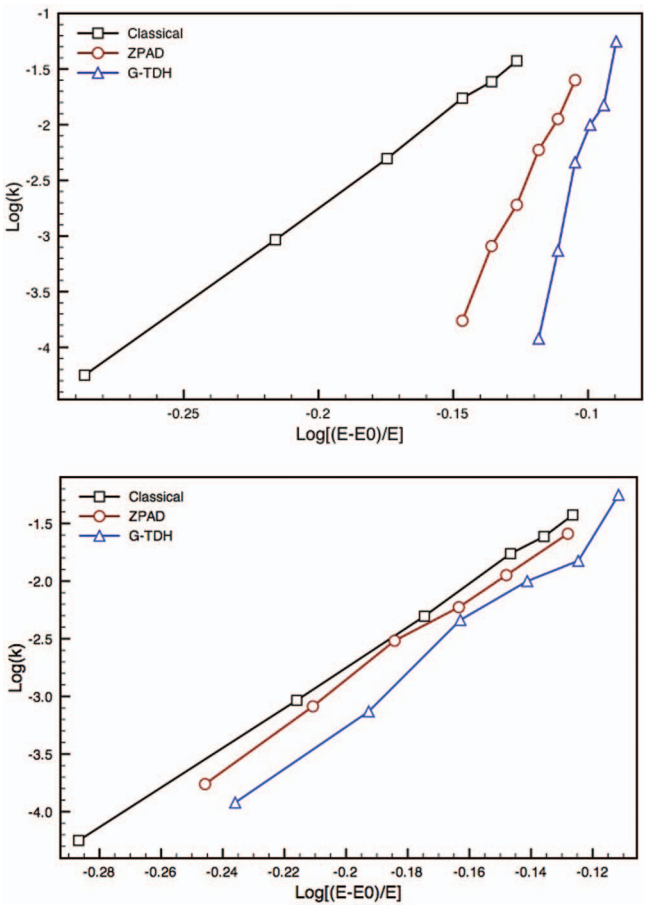

FIG. 5. Top panel: $\log_{10}(k_{diss})$ versus $\log_{10}[\frac{E_{int}-E_0}{E_{kin}}] = \log_{10}[\frac{E_{int}^{\text{Class}}-\Delta_0^{\text{Class}}}{E_{int}^{\text{Class}}}]$ for Ne_8, with $E_{int}^{\text{Class}} - \Delta_0^{\text{Class}}$ being the maximum internal energy available for the daughter cluster Ne_7. Bottom panel: $\log_{10}(k_{diss})$ versus $\log_{10}[\frac{E_{int}^X-\Delta_0^X}{E_{int}^X}]$ for Ne_8, with $E_{int}^X - \Delta_0^X$ being the maximum internal energy available for the daughter cluster Ne_7 for X = classical (black line, squares), ZPAD (red line, circles), or G-TDH (blue line, triangle), simulation method. Rates in ps^{-1}, energies in cm^{-1}.

which brings them in much better agreement with the classical ones. This change up to two orders of magnitude in the ZPAD and G-TDH rates comes from the reduction of E_{int}^X and Δ_0^X for these methods compared to the classical quantities. For instance, Δ_0^{ZPAD} is lower than Δ_0^{Class} (93.7 cm^{-1}) by 30%–40% in the energy range explored. The decrease in Δ_0 for G-TDH is even larger (roughly 50%). Given the somewhat limited amount of kinetic energy available (153.6–241.4 cm^{-1}) to both classical and ZPAD clusters in the energy range studied, and the large number of internal degrees (21) of freedom over which it is distributed (the average kinetic energy per degree of freedom is roughly 7.3–11.5 cm^{-1}), it is not surprising that the different Δ_0 values can induce a substantial difference in the dissociation rates.

The minor discrepancy remaining between the classical, ZPAD, and G-TDH curves in the bottom plot of Fig. 5 can be attributed to different effects of the anharmonicity, which is expected to increase the density of states more in the ZPAD case than in the others.[21,51] The shallower (and more anharmonic) pair interaction used in ZPAD simulations allows wider fluctuation than in the classical case for a given value of the internal energy, thus letting the system explore a larger volume of the phase space. This idea is supported by the fact that fitting the data shown in Fig. 5 with the usual RRK form $k_{diss} = \nu(\frac{E_{int}-\Delta_0}{E_{int}})^{s-1}$ provides one with a fairly accurate representation of their behaviour as a function of E_{int}; the most appropriate (i.e., the *effective*) value for s, the number of active degrees of freedom, is in both cases ($s_{\text{ZPAD}} = 19.4$ and $s_C = 18.6$) slightly higher than the theoretical one, $s = 18$. This finding can be interpreted[51] as indicating a faster growth of the number of states for the ZPAD generalized transition state compared to the density of state for the ZPAD reactant than in the classical case, in the framework of the transition state theory. This comes from the shallower well, lower dissociation energy and longer pair equilibrium distance in ZPAD species, which lead to stronger anharmonic behaviour compared to the classical case. The analysis of the G-TDH results is not as straightforward since the Gaussian width is variable, and hence the dynamics cannot be described by an effective potential. However, the width of the surface atoms varied in a fairly homogeneous way over the time needed to escape the cluster. Hence, the interpretation of the residual difference with classical dynamics is similar to that in the ZPAD case.

Similar conclusions can be reached from the classical and ZPAD results presented in the supplementary material for Ne_{13}, Ne_{14}, and Ne_{19}.

C. Capture probabilities

In Sec. III B it was shown that the different amounts of kinetic energy available for the vibrational and rotational motion of Ne_n obtained in the different simulation methods have a major influence on the dynamics. For a given total energy, a cluster could be considered as "colder" than in classical simulations when either the ZPAD or the G-TDH method is used. Such difference may also have an effect in the case of post-collisional capture. Indeed, a colder cluster can be more efficient as an energy "sink" as shown in the detailed analysis of post-collision capture for classical Ar_n species.[16] However, there is a competing effect in the case of quantum clusters. A weaker effective pair interaction (in the ZPAD case) or a less efficient energy redistribution due to more sparse energy states[52] will make energy transfer less efficient. It seems therefore interesting to us to investigate such a case in some depth.

1. Classical and ZPAD results

Figure 6 shows the capture probability obtained by employing classical trajectories and ZPAD ones for Ne_8 at two different target energies, namely $E = -285.3$ and -241.4 cm^{-1}. For these two energies, evaporation lifetime is much larger than the duration of the capture event, see Table II: not a single dissociation event was recorded in 4000 G-TDH trajectories. The relative impact velocities were $v_p = 4.17$ and 8.34 bohrs ps^{-1} (corresponding to a relative kinetic energy of 39.98 and 159.93 cm^{-1}). The first one is

Downloaded 02 Jul 2012 to 193.205.162.64. Redistribution subject to AIP license or copyright; see http://jcp.aip.org/about/rights_and_permissions

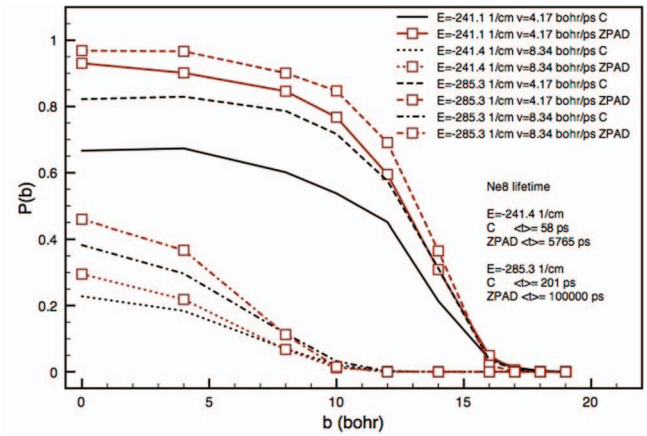

FIG. 6. Capture probability $P_s(n, b, E, v_p)$ as a function of the impact parameter b for Ne_8, computed using two different values of the cluster total energy, two projectile-target relative velocities and both classical (C) and ZPAD simulations. Average capture probabilities computed employing 2000 trajectories. A projectile was considered captured after the projection of its velocity on the line joining its center of mass with the cluster one had changed sign 5 times. Notice that both values of the cluster energy were sufficiently low to eliminate the chance for a dissociation event before a collision could take place.

close to the maximum of the Maxwell–Boltzmann distribution for Ne at ~70 K. The second is in the high speed tail with a probability about 10 times lower. Its corresponding kinetic energy is roughly twice the well depth of the effective pair interaction and 20% larger than the classical well depth. Hence, the relative collision energy is substantial compared with the average internal energy per degree of freedom, roughly 15.9–18.4 cm^{-1} in the classical case.

As expected, Fig. 6 shows a substantially lower capture probability for high speed projectiles for all values of the impact parameter b. It also shows that higher cluster internal energies give lower P_s, with a larger relative change in classical simulations for a high speed projectile. Also, the ZPAD method gives substantially higher capture probabilities, especially for the more energetic targets ($E = -241.4$ cm^{-1}). This finding indicates that the simple concept of "colder" clusters is winning over the weaker target-projectile interactions in the quantum mechanical effects over sticking probabilities.

It is also interesting to note that both classical and ZPAD simulations give similar values of P_s at large values of b for a given (E,v_p) pair. This finding is probably due to the fact that $u_{eff}(r_{jk})$ differs from the classical pair potential mainly in the well region, while its shape at large b is only slightly affected by the Gaussian "smearing" of the particle wave function. For ZPAD, a value of $\alpha \geq 1.5$ a.u. (width $\delta = \alpha^{-1/2} \leq 0.82$ bohrs) characterizes the cluster and projectile atoms. In other words, the potential experienced by a projectile during a glancing collision is very much the same for both methods. Overall, the classical and ZPAD data provided in the supplementary material for Ne_{13}, Ne_{14}, and Ne_{19} fully support this discussion.

2. G-TDH results, frozen width projectile

The G-TDH method was also used to investigate the influence of quantum effects on the capture process. As a first experiment, we opted for freezing the projectile width parameter α_{proj} ($\beta_{proj} = 0$ in Eq. (6)), while propagating the width parameters of the target atoms. Since the capture probability is expected to depend on α through the effective projectile-target atoms interaction potential, we ran calculations for a range of α_{proj} values, in order to help interpreting the results obtained further down with a variable projectile width. This way we can see how quantum target cluster atoms differ from classical ones (at the mean field level) in absorbing part of the collisional energy and temporarily forming a metastable energized species. This is one step up from the ZPAD approach which, although including zero point effects in an average sense, still remains fundamentally classical with respect to energy exchange. G-TDH is expected to incorporate at least some of the changes in the wave function induced during a collision. In particular, it is expected to correctly describe the compression of atomic functions upon collision.

The top panel of Fig. 7 shows the results for three sets of such calculations for Ne_8 at -285.3 cm^{-1} and $v_p = 4.17$ bohrs ps^{-1}. The results obtained using the ZPAD approach under the same conditions are also shown for comparison.

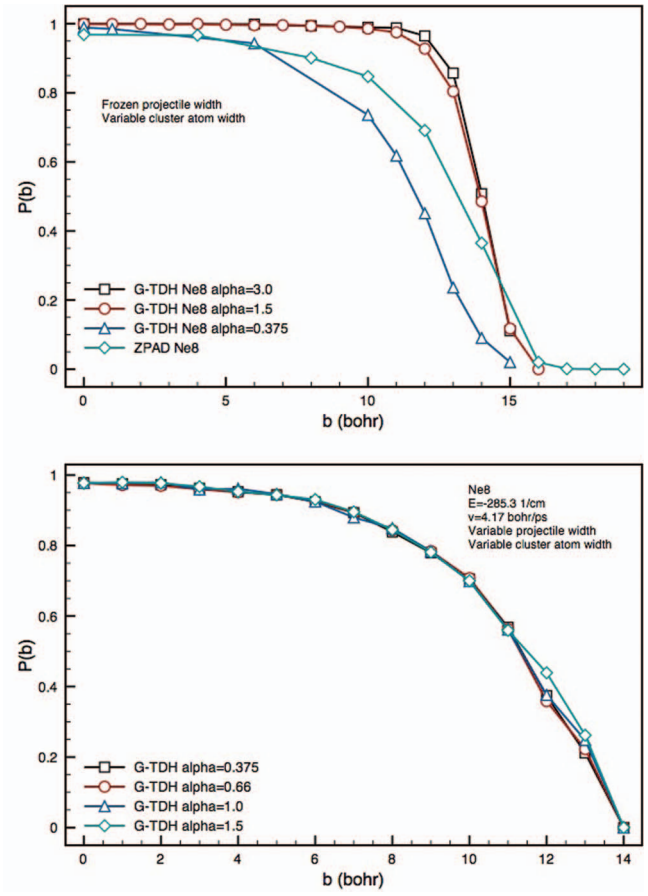

FIG. 7. Capture probability $P_s(n, b, E, v_p)$ as a function of the impact parameter b for Ne_8, computed using the G-TDH approach. Top panel: the width of the projectile was kept frozen at the value indicated in the picture, whereas the width of the cluster atoms is allowed to adapt. ZPAD results also shown for comparison. Bottom panel: G-TDH calculations employing a q value (see main text) for which the projectile width is activated in at least 90% of the trajectories. In all cases, $E = -285.3$ cm^{-1} and $v = 4.17$ bohrs ps^{-1}.

Downloaded 02 Jul 2012 to 193.205.162.64. Redistribution subject to AIP license or copyright; see http://jcp.aip.org/about/rights_and_permissions

Figure 7 shows that the G-TDH method gives higher capture probabilities than ZPAD (frozen Gaussian for all atoms with $\alpha = 1.66$ a.u., or $\delta = 0.776$ bohrs) over a large range of impact parameters ($b < 15$ bohrs) when the width of the projectile Gaussian is small, i.e., when the projectile is nearly classical. In this case, the "colder nature" of a G-TDH-described cluster accounts for the results. Also, the decay of the capture probability upon increasing b in the G-TDH simulation with $\alpha_{proj} = 1.5$ and 3.0 a.u. ($\delta = 0.82$–0.58 bohr) is sharper than with the ZPAD approach that, in turn, gives a sharper drop than classical trajectories. When using a wider projectile Gaussian ($\alpha_{proj} = 0.375$ a.u., $\delta = 1.63$ bohrs), the sticking probability is lower than both the ZPAD results and the G-TDH ones obtained with high α_{proj} values, a fact clearly evident at large b values. This can be explained by the fact that a wider Gaussian for the projectile raises the bottom of the effective potential well (e.g., see Fig. 3) and induces the onset of the repulsive wall at larger interatomic distances. Conversely, a narrow width corresponds to a deeper well due to a narrower averaging range. Notice that, around $b = 0$, $P_s(b)$ is insensitive to the Gaussian width. In that region, there is enough relative energy in the collision for the projectile to experience the repulsive wall of the cluster-atom potential, so that energy exchange is mainly similar to "hard sphere knock"-type collisions, with substantial disregard to the G-TDH widths. It is, clearly, at the outskirt of a cluster where differences in the interaction potential due to a different width can play a substantial role in defining the capture probability.

Despite the differences in the onset of the decay and in the absolute value of $P_s(b)$, both ZPAD and G-TDH computed $P_s(b)$ decay toward zero in the same range of impact parameters, $10 \geq b \geq 15$ bohrs. This range is consistent with the size of Ne_8 and the location of the minimum in the effective pair potential. The classical capture probabilities also decay in the same b range, indicating the common origin of this feature. A direct comparison with classical simulations (see Fig. 6) shows that G-TDH sticking probabilities are higher than classical ones over the whole range of impact parameters when narrow initial widths are used. For $\alpha_{proj} = 0.375$ a.u. ($\delta = 1.63$ bohrs) this is true only at low b values.

This suggests the existence of two different regimes: low ($b \lesssim$ cluster radius) impact parameters which is dominated by highly sticking "hard-knock" type collisions that are quite insensitive to the effective potential depth, and high ($b \gtrsim$ cluster radius) impact parameters where the sticking probability strongly depends on the potential attraction and hence on the α value. At low impact parameters G-TDH gives higher $P_s(b)$ because the G-TDH cluster is even "colder" than the ZPAD one, which favors energy exchange between cluster and projectile. At high impact parameters the same effect is at play, but it can be compensated by a smaller potential attraction for larger α_{proj} values.

Needless to say, the lowest value of $\alpha_{proj} = 0.375$ a.u. used in the G-TDH simulations ought to be considered largely unphysical when compared with the width associated to atoms in a cluster such as a metastable Ne_9^* formed during a sticking collision, ($1.7 < \alpha < 2.5$ a.u., or $0.63 \leq \delta \leq 0.76$ bohr), if it is assumed that the latter survives long enough to statistically redistribute the excess energy. Such conclusion can be inferred from our description on the dependency of α with respect to E (*vide supra*).

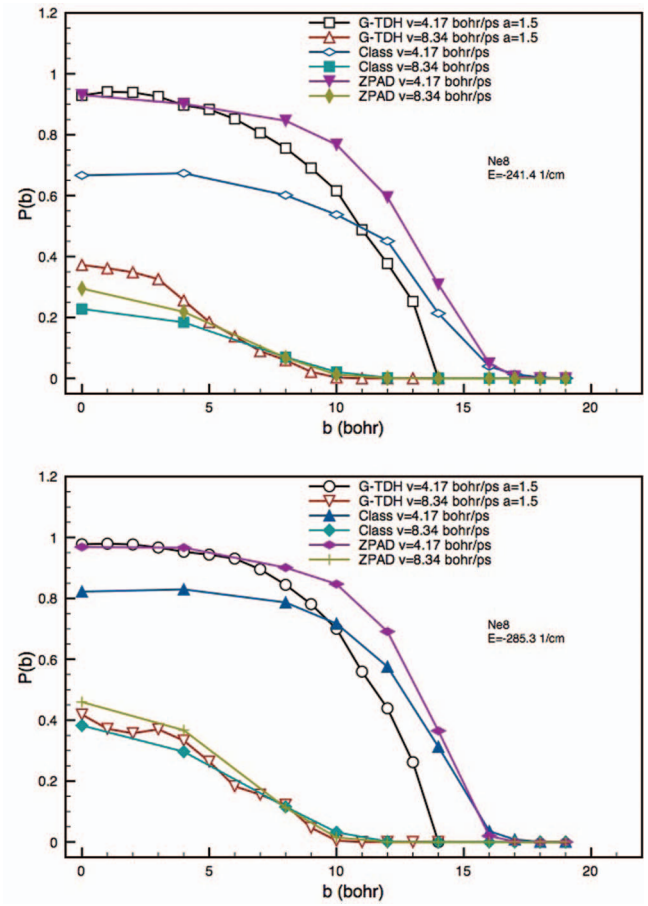

FIG. 8. Capture probability $P_s(n, b, E, v_p)$ as a function of the impact parameter b for Ne_8, computed using G-TDH with a dynamically adapting width for the projectile. Initially, $\alpha = 1.5$ in all calculations; q was chosen to have more than 90% of trajectories activating width adaptation. Also shown, there are the results obtained by classical (C) and ZPAD trajectories. Top panel, $E = 285.3$ cm^{-1}; bottom panel, $E = -241.4$ cm^{-1}.

3. G-TDH, variable projectile width

We now turn to investigating the changes induced by allowing the width of the projectile to dynamically adapt to its local environment and energy density. We have checked that P_b does not depend on the initial value chosen for α_{proj} if q (defined in Eq. (9)) is chosen to have more than 90% of trajectories with the projectile width adaptation activated (see Sec. II D and bottom panel of Fig. 7).

As shown in Fig. 8, G-TDH gives higher sticking probabilities than classical mechanics for $b < 10$, which is the range of hard sphere type collisions. This is consistent with the results found employing the ZPAD method. In this range, the quantum clusters are colder and can more easily dissipate the collision energy. For the high impact parameter range, we found classical dynamics to be more efficient for sticking than G-TDH, indicating a weaker attraction in the quantum case. This is different from the ZPAD and the frozen projectile G-TDH ($\alpha_{proj} = 1.5$ and 3) methods, which predict higher sticking probabilities than the classical ones. This surprising result can be explained as follows. In this range of

Downloaded 02 Jul 2012 to 193.205.162.64. Redistribution subject to AIP license or copyright; see http://jcp.aip.org/about/rights_and_permissions

TABLE III. Capture cross section $\sigma(n, E_{int}, v_p)$ (in bohr^2) as a function of the cluster energy E (in cm^{-1}) and the projectile speed v_p (in bohr ps^{-1}) for Ne_8 computed using classical trajectories, ZPAD dynamics and G-TDH.

	$\sigma(8, E, v_p)$		
(E,v_p)	Classical	ZPAD	G-TDH
(−285.3,4.17)	436.3	506.5	388
(−285.3,8.34)	51.0	55.2	53.3
(−241.4,4.17)	336.3	462.6	351.5
(−241.4,8.34)	31.6	33.5	38.6

large impact parameter, the sticking probability is governed by the long range attractive part of the cluster-projectile interaction. In the case of G-TDH, the Gaussian wave packet is spreading in this region which results in a smaller attraction. This effect is strong enough to counterbalance the lower "temperature" of the target cluster due to quantum effects.

4. Capture cross sections

To provide a more global quantitative measure of the difference between classical and ZPAD simulations, we have computed the capture cross sections for the cases shown in Figs. 6 and 8. This was performed by computing numerically the integral

$$\sigma(n, E_{int}, v_p) = \int_0^\infty db\, b P_s(n, b, E_{int}, v_p), \qquad (14)$$

using the trapezoidal rule and the data shown in Figs. 6 and 8. The results are displayed in Table III.

As for capture probabilities, the difference between classical and ZPAD capture cross sections is larger for higher energies (roughly 15% at $E = -285.3$ cm^{-1} compared to roughly 30% at $E = -241.4$ cm^{-1}) and for the lower projectile collision speed, whereas the cross section given by G-TDH is 12% lower than classical trajectories at $E = -285.3$ cm^{-1} and 4% higher at $E = -241.4$ cm^{-1}. Notice that these differences are due to a slower decrease of the ZPAD and G-TDH σ upon increasing E compared to classical σ. This is due to the fact that u_{eff} becomes shallower upon increasing E (see Fig. 3). This in turn implies a slower increase of the internal energy in the ZPAD and G-TDH targets. At higher v_p, the difference between classical, ZPAD and G-TDH is roughly the same for the two different values of E. In our view, this is the result of two counterbalancing effects, namely the fact that the major effect on P_s is the kinetic energy of the projectile (its value is much higher than the average kinetic energy available per internal degree of freedom), and the b-weighting of the sticking probabilities, which gives more importance to higher impact parameter regions where P_s is largely independent of the simulation method employed.

IV. DISCUSSION AND CONCLUSIONS

In this work, we investigated quantum mechanical effects on the quantitative description of rare gas cluster dissociation and projectile capture, two key steps in the description of homogeneous nucleation in the gas phase. Given the many-body nature of the systems involved, we had to resort to approximate methods, ZPAD and G-TDH, in our exploration. The G-TDH method contains the key ingredients needed for a correct quantum description, namely, a reasonably accurate treatment of the ZPE and single particle wave functions that correctly adapt their width to the local interactions as the process evolves. Thus, our results, although not strictly exact, should be expected to give a correct quantum mechanical description.

The results obtained with quantum methods for Ne_n differ from the ones produced by classical trajectories because of the effect of zero point motion, which substantially reduces the available energy content in the quantum case. As stressed in Ref. 57, it is standard practice in classical simulations *not* to add zero-point energy in the initial conditions, because it could lead the system to explore regions of phase space completely ignored by quantum mechanics. In our case, capture probabilities are enhanced for quantum clusters compared to classical ones for the ZPAD and frozen projectile width G-TDH methods. This is a direct indication that quantum effects "cool" the target cluster, in the sense that less kinetic energy is available to each degree of freedom. This favors energy relaxation of the projectile in the target internal modes. In practice, we found the capture cross sections to be increased by 15%–30% in a quantum cluster with respect to a classical one when the projectile impact speed corresponds to the average for Ne gas at 70 K. These considerations are also true for G-TDH. However, in this case the spreading of the projectile wave function makes the cluster-projectile attraction less efficient. This leads to lower total capture cross sections because of the high weight of the large impact parameter region in the total cross section. In addition, we showed that the cross section is less sensitive to an increase of the cluster internal energy or "temperature" when using quantum methods rather than the classical one.

The quantitative impact of a quantal description is strikingly more evident in the case of dissociation, with lifetimes that differ by a factor of 20–200 over the explored energy range. The difference between quantum and classical unimolecular dissociation rates has been discussed in the framework of RRKM theory by, e.g., Hase and Buckowski.[56] When zero-point energy is included in a classical dynamics simulation, it is allowed to move freely between all the degrees of freedom and can thus induce a non-physical dissociative event. The authors have compared the ethyl unimolecular dissociation rate constant obtained using the classical and vibrationally adiabatic quantal expressions of the semi-empirical Whitten-Rabinovitch approximation.[58] The classical rates are higher and the difference decreases with increasing total energy, as expected since the relative weight of the zero-point energy decreases. Comparing dissociation rates with the same total energy (this work) amounts to including the zero-point energy in the classical simulation. In our case, the classical simulations indeed suggest a faster dissociation process. This is interesting because the energy required to dissociate one atom is lower in the quantum simulation than in the classical one.

Downloaded 02 Jul 2012 to 193.205.162.64. Redistribution subject to AIP license or copyright; see http://jcp.aip.org/about/rights_and_permissions

Amazingly, the large differences in k_{diss} obtained by the different methods could be reconciled by means of simple concepts borrowed from transition state theory, namely the effective dissociation barrier (approximated by the dissociation energy Δ_0 for one monomer) and the maximum amount of internal energy available to the daughter cluster. This is clearly a novel finding.

We now discuss the consequences of our findings on the time evolution of a condensing system. Our dissociation rate data suggest that the quantum metastable clusters survive longer, making it more likely for a collision with another body to quench their energy content (recall that metastable pre-critical clusters are likely to be highly energized species). This suggests that quantum species should be expected to nucleate and condense faster than classical ones. This conclusion is also supported by the capture results given in Table III. The two results at the higher energy $E = -241.4$ cm^{-1} are of particular relevance for the initial stages of the nucleation, which are expected to be highly "out of equilibrium." The quantum capture cross section is higher than the classical one. This is of high relevance; whether this translates into faster quantum nucleation rates remains to be tested by comparing collisional energy exchange efficiency for quantum and classical systems. The "continuous energy" nature of classical mechanics could lead to third body collisions being more efficient in stabilizing "hot" species, and this could invert the tendency of the quantum effects for capture and dissociation. However, such possibility needs to be verified by means of a full simulation of a nucleation process via a statistical approach.[17] This will be the subject of future work.

Some of our conclusions can be extended to molecular species. Zero-point effects should play the same role, with the intramolecular modes added. The relative contribution of translations and rotations should depend largely on the structural details of the molecules, the strength of their interaction as well as the isotopic composition even for small rigid species such as ammonia.[53–55] It would thus be interesting to investigate zero-point energies and quantum averaged structures for large molecular clusters, in order to extract useful information on the parents and daughters in monomer capture and dissociation. In addition, molecular dissociation can exhibit an entropic effect that is not present in atomic clusters. The orientation of the leaving monomer becomes free at or near the transition state, which increases entropy. This could compensate the gain in free energy in the quantum simulations.

The G-TDH method has proved to be a useful tool to describe the dissociation process in atomic clusters. The flexibility of the atom wave function allowed us to show that the more approximate ZPAD method contains all the basic ingredients needed for a reasonable description of such process. Hence the ZPAD method can be used to describe capture and dissociation in other similar systems, as well as for including some quantum effects in the description of cluster isomerization. The G-TDH method should be useful in simulations of particle collisions and energy exchange. Besides, a generalization to describe small molecular species would also be useful for future studies on molecular clusters. The G-TDH method can also be used for quantum systems whose constituents can be described by a compact wave function such as para-H_2 clusters and condensed phases. It should also be valid for the description of He droplets in the presence of strongly binding impurities capable of localizing He atoms in the first few solvation shells. The description of interesting processes such as energy and mass transport (e.g., after ionization or excitation) would then become approachable within the computing time affordable nowadays. Work in these directions is underway in our laboratories.

ACKNOWLEDGMENTS

M.M. acknowledges the financial support provided by the "Rientro dei Cervelli" scheme funded by the Italian Ministry for the University and Reserach (MIUR), a Visiting Research grant awarded by the Université Paul Sabatier, as well as the hospitality at the Laboratoire Collisions Agrégats Réactivité-CNRS. We also acknowledge the calculation facilities provided by CALMIP. N.H. acknowledges support from the French National Research Agency under Programme Blanc (ANR-08-BAN-0146-02, DYNHELIUM).

[1] J. T. Wescott, P. Kung, and A. Maiti, Appl. Phys. Lett. **90**, 033116 (2007).
[2] C. Bréchignac, P. Houdy, and M. Lahmani, *Nanomaterials and Nanochemistry* (Springer, Heidelberg, 2007).
[3] F. F. Abraham, *Homogeneous Nucleation Theory* (Academic, New York, 1974).
[4] J. W. P. Schmelzer, *Nucleation Theory and Applications* (Wiley-VHC, Weinhem, 2005).
[5] P. E. Wagner and G. Vali, *Atmospheric Aerosols and Nucleation* (Springer-Verlag, Berlin, 1998).
[6] M. Kulmala and P. E. Wagner, *Nucleation and Atmospheric Aerosols 1996* (Pergamon, Oxford, 1996).
[7] C. Desgranges and J. Delhommelle, J. Am. Chem. Soc. **133**, 2872 (2011).
[8] B. E. Wyslouzil and J. H. Seinfeld, J. Chem. Phys. **97**, 2661 (1992).
[9] J. Wedekind and D. Reguera, J. Chem. Phys. **127**, 154516 (2007).
[10] S. Toxvaerd, J. Chem. Phys. **115**, 8913 (2001).
[11] K. K. Tanaka, K. Kawamura, H. Tanaka, and K. Nakazawa, J. Chem. Phys. **122**, 184514 (2005).
[12] H. Matsubara, T. Koishi, T. Ebisuzaki, and K. Yasuoka, J. Chem. Phys. **127**, 214507 (2007).
[13] J. Merikanto, E. Zapadinsky, A. Lauri, and H. Vehkamaki, Phys. Rev. Lett. **98**, 145702 (2007).
[14] F. Trudu, D. Donadio, and M. Parrinello, Phys. Rev. Lett. **97**, 105701 (2006).
[15] J. Julin, I. Napari, J. Merikanto, and H. Vehkamki, J. Chem. Phys. **133**, 044704 (2010).
[16] M. Mella, J. Chem. Phys. **131**, 124309 (2009).
[17] J. C. Barrett, J. Chem. Phys. **128**, 164519 (2008).
[18] J. W. Brady, J. D. Doll, and D. L. Thompson, J. Chem. Phys. **74**, 1026 (1981).
[19] G. K. Schenter, S. M. Kathmann, and B. C. Garrett, J. Chem. Phys. **116**, 4275 (2002).
[20] I. Napari, H. Vehkamäki, and K. Laasonen, J. Chem. Phys. **120**, 165 (2004).
[21] M. Mella, J. Chem. Phys. **130**, 084108 (2009).
[22] S. Weerasinghe and F. G. Amar, J. Chem. Phys. **98**, 4967 (1993).
[23] G. H. Peslherbe and W. L. Hase, J. Chem. Phys. **105**, 7432 (1996).
[24] C. D. Cappa, W. S. Drisdell, J. D. Smith, R. J. Saykally, and R. C. Cohen, J. Phys. Chem. B **109**, 24391 (2005).
[25] C. Vega, M. M. Conde, C. McBride, J. L. F. Abascal, E. G. Noya, R. Ramirez, and L. M. Sesé, J. Chem. Phys. **132**, 046101 (2010).
[26] J. M. Sorenson, J. K. Gregory, and D. C. Clary, Chem. Phys. Lett. **263**, 680 (1996).
[27] B. L. Hammond, W. A. Lester, Jr., and P. J. Reynolds, *Monte Carlo Methods in Ab Initio Quantum Chemistry*, 1st ed. (World Scientific, Singapore, 1994).
[28] P. Slavìčcek, P. Jungwirth, M. Lewerenz, N. H. Nahler, M. Farnik, and U. Buck, J. Phys. Chem. A **107**, 7743 (2003).

Downloaded 02 Jul 2012 to 193.205.162.64. Redistribution subject to AIP license or copyright; see http://jcp.aip.org/about/rights_and_permissions

[29]D. Bonhommeau, M. Lewerenz, and N. Halberstadt, J. Chem. Phys **128**, 1 (2008).
[30]E. J. Heller, J. Chem. Phys. **75**, 2923 (1981).
[31]See supplementary material at http://dx.doi.org/10.1063/1.4730033 for results on clusters larger than Ne_8.
[32]P. Håkansson, M. Mella, D. Bressanini, G. Morosi, and M. Patrone, J. Chem. Phys. **125**, 184106 (2006).
[33]P. Håkansson and M. Mella, J. Chem. Phys. **126**, 104106 (2007).
[34]S. Chiesa, M. Mella, G. Morosi, and D. Bressanini, J. Chem. Phys. **119**, 5601 (2003).
[35]P. Slavìček and M. Lewerenz, Phys. Chem. Chem. Phys. **12**, 1152 (2010).
[36]M. Mella, G. Morosi, and D. Bressanini, Phys. Rev. E **61**, 2050 (2000).
[37]R. A. Aziz and M. J. Slaman, Chem. Phys. **130**, 187 (1989).
[38]J. C. Barrett, J. Chem. Phys. **126**, 074312 (2007).
[39]J. W. Brady, J. D. Doll, and D. L. Thompson, J. Chem. Phys. **73**, 292 (1980).
[40]J. W. Brady, J. D. Doll, and D. L. Thompson, J. Chem. Phys. **71**, 2467 (1979).
[41]T. Yan, W. L. Hase, and J. C. Tully, J. Phys. Chem. **120**, 1031 (2004).
[42]H. W Schranz, L. M. Raff, and D. L. Thompson, J. Chem. Phys. **94**, 4219 (1991).
[43]S. Severin, B. C. Freasier, N. D. Hamer, D. L. Jolly, and S. Nordholm, Chem. Phys. Lett. **57**, 117 (1978).
[44]M. Sterling, Z. Li, and V. A. Apkarian, J. Chem. Phys. **103**, 5679 (1995).
[45]F. Russo, Jr. and E. Curotto, J. Chem. Phys. **118**, 6808 (2003).
[46]P. A. M. Dirac, Proc. Cambridge Philos. Soc. **26**, 376 (1930).
[47]J. Frenkel, *Wave Mechanics* (Clarendon, Oxford, 1934).
[48]D. J. Wales, J. P. K. Doye, A. Dullweber, M. P. Hodges, F. Y. Naumkin, F. Calvo, J. Hernández-Rojas, and T. F. Middleton; see http://www-wales.ch.cam.ac.uk/CCD.html for a data base of cluster structures, energies, and interaction potentials.
[49]F. Calvo and P. Parneix, J. Chem. Phys. **126**, 034309 (2007).
[50]In principle $\Delta_0^{\mathrm{ZPAD}} = E_0^{\mathrm{ZPAD}}(n-1) - E_0^{\mathrm{ZPAD}}(n)$ should be calculated using $u_{eff}(r_{jk})$ of the parent cluster for $E_0^{\mathrm{ZPAD}}(n)$ and $u_{eff}(r_{jk})$ of the daughter cluster for $E_0^{\mathrm{ZPAD}}(n-1)$. However this is impractical since the daughter internal energy depends on the kinetic energy release upon dissociation. Since the $u_{eff}(r_{jk})$ well depth was shown to depend only weakly on E_{int} (see Fig. 3), we opted for using $u_{eff}(r_{jk})$ of the parent cluster also for $E_0^{\mathrm{ZPAD}}(n-1)$.
[51]K. Song and W. L. Hase, J. Chem. Phys. **110**, 6198 (1995).
[52]L. E. B. Börjesson, S. Nordholm, and L. L. Andersson, Chem. Phys. Lett. **186**, 65 (1991).
[53]C. Lubombo, E. Curotto, P. Janeiro Barral, and M. Mella, J. Chem. Phys. **131**, 034312 (2009).
[54]E. Curotto and M. Mella, J. Chem. Phys. **133**, 214301 (2010).
[55]M. Patrone and M. Mella, Chem. Phys. Lett. **514**, 16 (2011).
[56]W. L. Hase and D. G. Buckowski, J. Comput. Chem. **3**, 335 (1982).
[57]W. L. Hase, C. L. Darling, and L. Zhu, J. Chem. Phys. **96**, 8295 (1992).
[58]P. J. Robinson and K. A. Holbrook, *Unimolecular Reactions* (Wiley-Interscience, New York, 1972).

Downloaded 02 Jul 2012 to 193.205.162.64. Redistribution subject to AIP license or copyright; see http://jcp.aip.org/about/rights_and_permissions